

## Numerical simulation of axis-ratio effects on forced convection heat transfer around the triangular unit of isothermal rectangular obstacle

Hadi Pourziaei Araban<sup>1</sup>, Javad Alinejad<sup>\*1</sup>, Davood Domiri Ganji<sup>2</sup>

<sup>1</sup>Department of mechanical engineering, Sari branch, Islamic Azad University, Sari, Iran

<sup>2</sup>Department of mechanical engineering, Babol Noshirvani University of Technology, Babol, Iran

Received: February 2021, Accepted: June 2021

### Abstract

The Lattice Boltzmann method (LBM) is employed to simulate heat transfer in flow past three arrangements of and horizontal and vertical rectangular obstacle under isothermal boundary condition. A thermal lattice Boltzmann BGK model is purposed to simulate the two dimensional forced convection for the governing parameters as Reynolds number,  $Re=100$  and the Prandtl Number for laminar flow  $Pr = 0.71$ . Pressure distributions, isotherms and streamlines were obtained. Vortex shedding maps are observed in detail for various cases and signified that lattice Boltzmann method can be effectively used to capture velocity fluctuations. The present results are in good agreement with existing experimental and numerical data.

\* Corresponding author; E-mail: Alinejad\_javad@yahoo.com, Alinejad\_javad@iausari.ac.ir

**Keywords:** lattice Boltzmann model; isothermal rectangular; Vortex shedding; Reynolds number

### 1. Introduction

The problem of forced convection has been a major topic of research since the starting point, due to its occurrence in industrial and technological applications, such as electronic cooling. Heat transfer has been considered by many researchers for different industrial applications. The flow of fluids past cylinders of various cross sections has been a challenge and an interesting problem to researchers [1-3]. Bluff body flows constitute an important class of problems within the domain of fluid mechanics. The elliptical cylinder is also one of the important bluff objects referred in Computational Fluid Dynamics field in which the aspect ratio and the angle of attack are the most important parameters [4]. It is also known that, elliptical cylinders offer less flow resistance and higher heat transfer rates than circular cylinders. In the recent decades, the Lattice Boltzmann method (LBM) has proved its capability to simulate a large variety of fluid flows. For the isothermal fluid flows, the LBM was found to be an accurate, stable and computationally economical method compared with classical computational fluid dynamics methods. The Lattice Boltzmann equation represents the minimal form of Boltzmann kinetic equation [5]. Control the temperature fluctuation in two-phase cuo-water Nano fluid by transfiguration of the enclosures. [6]. The main limitation of using LBM in engineering

applications is the lack of satisfactory model for the thermal fluid flows problems. The multi speed approach consists in extending the distribution function in order to obtain the macroscopic temperature [7, 8]. However, this approach requires much more computational effort due to the additional discrete speeds and suffers from numerical instabilities. For the passive scalar approach, it consists in solving the velocity by the LBM and the macroscopic temperature equation independently. The macroscopic temperature equation is similar to a passive scalar evolution equation if the viscous heat dissipation and compression work done by pressure are negligible. The coupling to LBM is made by adding a potential to the distribution function equation [9, 10]. From the other point of view, fluid flow around obstacles mounted on sheet forms a fundamental basis for study of the convective cooling of electrical devices and heat transfer. This interest was motivated by the rapid advances in electronic technology, with the trends of the electronic industry being oriented toward the development of more and more compact and powerful computers. This subject has received much attention, as electronic system and device technology has improved, and performance increases are sought. Korichi and Oufer [11] carried out a numerical investigation of flow field and heat transfer enhancement in a channel containing three obstacles; two attached to the lower wall and one to the upper wall. The results showed that transition from steady to unsteady flow occurs at lower values of Reynolds number, when compared to the channel with obstacles attached only to the lower wall. A study in steady flow regime for two circular cylinders in tandem arrangement, at four different Prandtl Numbers ( $Pr=0.1, 1, 10$  and  $100$ ) has been reported recently by Juncu [12]. A numerical simulation of forced convective incompressible flow in a horizontal plane channel and heat transfer over two isothermal tandem square cylinders has been carried out by Farhadi et al. [13, 14] using the finite-volume and LBM method. Their study details the effects of gap between two squares, Reynolds numbers ranging from 100 to 1000 and blockage ratio, on the characteristics of flow field and heat transfer. The present study emphasizes the implementation of LBM for the simulation of flow field and heat transfer around the isothermal cylinders to compare its results with results obtained by the finite element solution of Navier–Stokes and energy equation. The simulation is conducted at Prandtl Number of 0.71 and different Reynolds numbers,  $Re=100$ . Evaluation of the heat transfer rate increases in retention pools nuclear waste [15]. Several researches have been carried out using Lattice Boltzmann method, and by placing obstacles within the channels, heat transfer has been investigated which can be named as following. Fins arrangement and Nano fluids effects on three-dimensional natural convection in the cubical enclosure with numerical analysis [16]. Hybrid conduction, convection and radiation heat transfer simulation in a channel with rectangular cylinder researched by Peiravi [17]. Alinejad investigated analysis of secondary droplets characteristics due to drop impacting on 3d cylinders considering dynamic contact angle in numerical method [18]. Peirovi and society dissection 3D optimization of baffle arrangement in a multi-phase nanofluid natural convection based on numerical simulation. International Journal of Numerical Methods for Heat and Fluid Flow [19].

## 2. Lattice Boltzmann method

### 2.1. Governing equation

The lattice kinetic theory and especially the lattice Boltzmann method have been developed as significantly successful alternative numerical approaches for the solution of a wide class of problems [19–22]. The LBM is derived from lattice gas methods and can be regarded as a first order explicit discretization of the Boltzmann equation in phase space. This method (LBM) is a powerful numerical technique, based on kinetic theory, for simulating fluid flow [15, 18, 19] and heat transfer [25, 26],

and has many advantages in comparison with conventional CFD methods mentioned previously. In contrast with the classical macroscopic Navier–Stokes (NS) approach, the lattice Boltzmann method uses a mesoscopic simulation model to simulate fluid flow [20]. It uses modeling of the movement of fluid particles to capture macroscopic fluid quantities, such as velocity and pressure. In this approach, the fluid domain is made discrete in uniform Cartesian cells, each one of which holds a fixed number of Distribution Functions (DF) that represent the number of fluid particles moving in these discrete directions. Hence depending on the dimension and number of velocity directions, there are different models that can be used. The present study examined two-dimensional (2-D) flow and a 2-D square lattice with nine velocities (D2Q9 model). The velocity vectors,  $c_0 \dots c_8$ , of the D2Q9 model are shown in Figure1. For each velocity vector, a particle DF is stored. The velocities of the D2Q9 model are (Fig. 1) and temperature boundary condition for  $Re=100$  is shown in table 1:

$$c_k = \begin{cases} (0,0) & k = 0 \\ (\pm 1,0)c, (0, \pm 1)c & k = 1,2,3,4 \\ (\pm 1, \pm 1)c & k = 5,6,7,8 \end{cases} \quad (1)$$

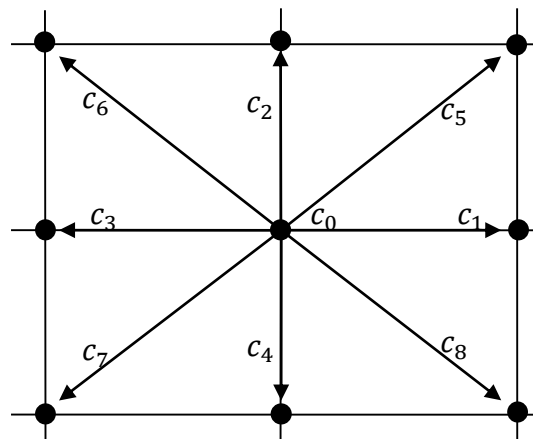


Fig. 1. 2-Dimensional for 9-velocity lattice (D2Q9) model

Table 1: Boundary condition

$Re_{in} = 100$	$T_{obstacle\ surface} = 1$	$T_{wall} = 0$
-----------------	-----------------------------	----------------

All physical properties of the fluid are considered to be constant. The Prandtl Number is taken equal to 0.71. At the outlet for air; all gradients are assumed to be zero.

Where  $c = \Delta x / \Delta t$  and  $k$  is the Lattice velocity direction

The LB model (D2Q9) used in the present work is the same as the one which is employed in [14]. The DFs are calculated by solving the Lattice Boltzmann Equation (LBE), which is a special discretization of the kinetic Boltzmann equation. After introducing Bhatnagar–Gross–Krook (BGK) approximation, the Boltzmann equation can be formulated as below [27]:

$$f_k(x + c_k \Delta t, t + \Delta t) = f_k(x, t) + \frac{\Delta t}{\tau} [f_k^{eq}(x, t) - f_k(x, t)] \quad (2)$$

Where  $\Delta t$  denotes lattice time step,  $c_k$  is the discrete lattice velocity in direction  $k$ ,  $\tau$  denotes the lattice relaxation time and  $f_k^{eq}$  is the equilibrium DF in the direction of the lattice velocity. Equilibrium DFs are calculated as:

$$f_k^{eq} = \omega_k \rho \left[ 1 + \frac{\mathbf{c}_k \cdot \mathbf{u}}{c_s^2} + \frac{1}{2} \frac{(\mathbf{c}_k \cdot \mathbf{u})^2}{c_s^4} - \frac{1}{2} \frac{\mathbf{u}^2}{c_s^2} \right] \quad (3)$$

Where the weights  $\omega_k$  are  $\omega_k = 4/9$  for  $k = 0$ ,  $\omega_k = 1/9$  for  $k = 1, 2, 3, 4$  and  $\omega_k = 1/36$  for  $k = 5, 6, 7, 8$ ; and  $c_s = c_k/\sqrt{3}$  is the lattice speed of sound. The macroscopic fluid variable densities and velocities are computed as the first two moments of the distribution functions for each cell:

$$\rho = \sum_{k=0}^8 f_k, \quad \mathbf{u} = \frac{1}{\rho} \sum_{k=0}^8 f_k \mathbf{c}_k \quad (4)$$

This model is explained in more detail in [27]. For the temperature field the  $g$  distribution is as below:

$$g_k(\mathbf{x} + \mathbf{c}_k \Delta t, t + \Delta t) = g_k(\mathbf{x}, t) + \frac{\Delta t}{\tau_g} [g_k^{eq}(\mathbf{x}, t) - g_k(\mathbf{x}, t)] \quad (5)$$

The corresponding equilibrium DFs for fluid and solid, respectively, are defined as follows [18]:

$$g_k^{eq} = \omega_k T \left[ 1 + \frac{\mathbf{c}_k \cdot \mathbf{u}}{c_s^2} \right] \quad (6)$$

$$g_k^{eq} = \omega_k T \quad (7)$$

The temperature field is computed as:

$$T = \sum g_k \quad (8)$$

## 2.2. Force and heat transfer evaluation

Heat transfer between hot and cold walls was computed by local and mean Nusselt number for is given as

$$Nu_l = - \left. \frac{\partial T}{\partial n} \right|_{wall} \quad (9)$$

$$Nu_m = \frac{1}{2\pi} \int_0^{2\pi} Nu_l d\theta \quad (10)$$

The two characteristic quantities of flow around a cylinder are the coefficient of drag and coefficient of pressure. That we use for validation (fig 2) The coefficients are defined as

$$C_D = \frac{F_D}{\frac{1}{2}\rho U_\infty^2 l} \quad (11)$$

### 2.3. Numerical procedure

The physical geometry considered in this study is shown in Fig. 3. As can be seen the horizontal and vertical rectangular are arranged in the triangular configuration. All channel dimensions are considered as long enough ones to ensure that the recirculation takes place inside the computational domain, and the outflow has no effect on the physical variables which are investigated.

The mentioned triangular unit is mounted inside a channel which is sufficiently wide in a way that its walls exert no measurable effect on the flow field characteristics. Moreover, the rectangular are assumed to be too long so that the ends effects are neglected. The temperature of the walls ( $T_c$ ) is equal to the temperature of the incoming fluid ( $T_\infty$ ) which is constant during the computation. As well, the temperature of the cylinders surfaces ( $T_h$ ) is assumed to be constant, however, higher than the incoming fluid temperature. In this study, three kinds of boundary conditions are applied; bounce back condition is handled on the surface of cylinders and channel walls to obtain no slip boundary condition, constant velocity and constant pressure are set at inlet and outlet boundaries, respectively. The bounce back this boundary conditions are performed as below,

At the up wall of the channel

$$f_7(x, t + \Delta t) = f_5(x, t), \quad f_4(x, t + \Delta t) = f_2(x, t), \quad f_8(x, t + \Delta t) = f_6(x, t)$$

and at the down wall of the channel

$$f_5(x, t + \Delta t) = f_7(x, t), \quad f_2(x, t + \Delta t) = f_4(x, t), \quad f_6(x, t + \Delta t) = f_8(x, t)$$

At the inlet of the channel the boundary condition with known velocity ( $u_{in}$ ) is applied (Fig. 3). In this position three unknown distribution function based on equation (3) are calculated.

Equation (3) at inlet boundary can be written as,

$$\rho = \sum_{k=0}^8 f_k \implies \rho_{in} = f_0 + f_1 + f_2 + f_3 + f_4 + f_5 + f_6 + f_7 + f_8 \quad (12)$$

$$\mathbf{u} = \frac{1}{\rho} \sum_{k=0}^8 f_k \mathbf{c}_k \xrightarrow{\text{for } x\text{-component}} \rho_{in} u_{in} = f_1 + f_5 + f_8 - f_3 - f_6 - f_7 \quad (13)$$

The equilibrium condition normal to the boundary, yields

$$f_1 - f_1^{eq} = f_3 - f_3^{eq} \quad (14)$$

where  $f^{eq}$  can be calculated from equation (2)

$$f_1^{eq} = \frac{1}{9} \rho_{in} \left[ 1 + 3u_{in} + \frac{9}{2} u_{in}^2 - \frac{3}{2} u_{in}^2 \right] \quad (15)$$

And

$$f_3^{eq} = \frac{1}{9} \rho_{in} \left[ 1 - 3u_{in} + \frac{9}{2} u_{in}^2 - \frac{3}{2} u_{in}^2 \right] \quad (16)$$

Substituting above equations in equation (18) yields,

$$f_1 = f_3 + \frac{2}{3} \rho_{in} u_{in} \quad (17)$$

The remaining unknown distribution functions are calculated by solving these equations as below,

$$\rho_{in} = \frac{(f_0 + f_2 + f_4) + 2(f_3 + f_7 + f_6)}{1 - u_{in}} \quad (18)$$

$$f_5 = f_7 - \frac{1}{2} (f_2 - f_4) + \frac{1}{6} \rho_{in} u_{in} \quad (19)$$

$$f_8 = f_6 + \frac{1}{2} (f_2 - f_4) + \frac{1}{6} \rho_{in} u_{in} \quad (20)$$

At the outlet the open boundary condition is performed. The applied approach is to assume that the pressure at this boundary is known i.e. density ( $\rho_{outlet}$ ). At the outlet three unknown distribution function are calculated as below,

$$u_x = -1 + \frac{(f_0 + f_2 + f_4) + 2(f_1 + f_5 + f_8)}{\rho_{outlet}} \quad (21)$$

$$f_3 = f_1 - \frac{2}{3} \rho_{outlet} u_x \quad (22)$$

$$f_7 = f_5 + \frac{1}{2} (f_2 - f_4) - \frac{1}{6} \rho_{outlet} u_x \quad (23)$$

$$f_6 = f_8 - \frac{1}{2} (f_2 - f_4) - \frac{1}{6} \rho_{outlet} u_x \quad (24)$$

### 3. Code Validation

The numerical simulation was done by an in-house code written in FORTRAN, using LBM. Numerical investigations were carried out for flow past a single square confined in a channel. The comparison of pressure distribution and drag coefficient with previous work at different Reynolds numbers (100,200) show that a very good agreement has been obtained in Fig. 2 is our drag coefficient report in Table(2

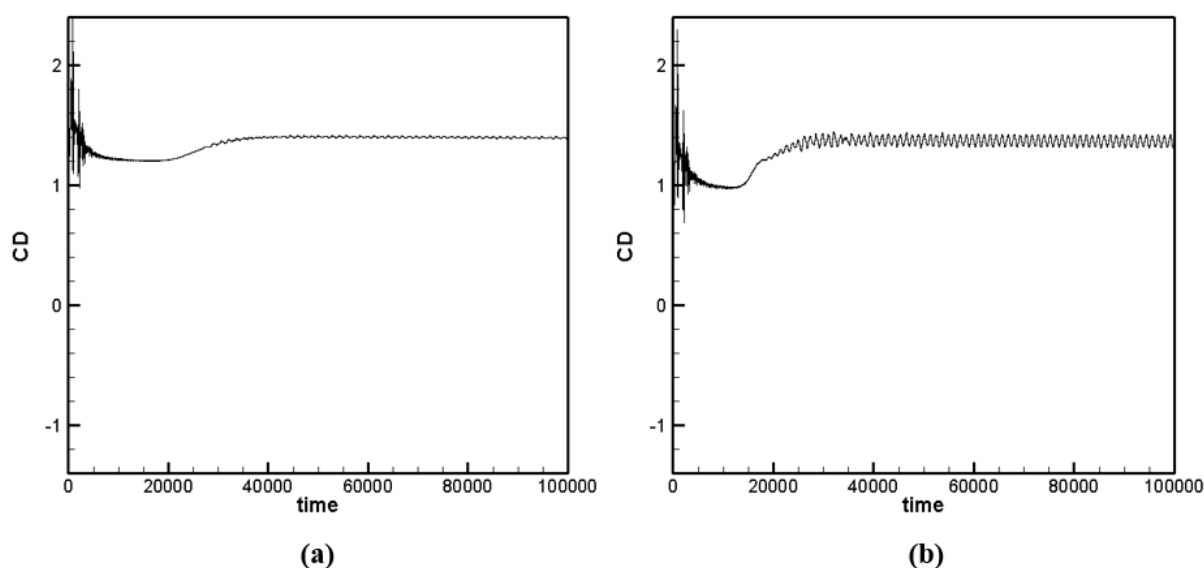


Fig. 2. Drag coefficient versus time step for (a)  $Re = 100$  , (b)  $Re = 200$

Table2 : Drag coefficient comparison

	Present study	Ref. [34]
$Re = 100$	1.401	1.51
	Present study	Ref. [35]
$Re = 200$	1.370	1.43

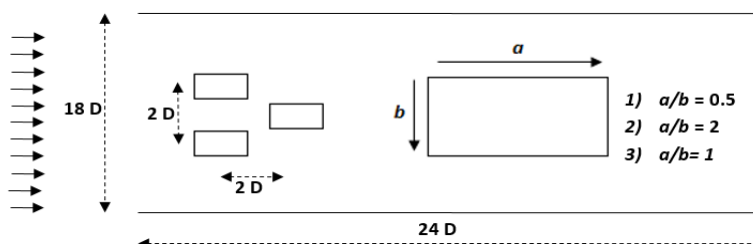


Fig. 3. Schematic diagram of the computational domain.

In the first section, three rectangles are placed horizontally, in order to studying the distribution of temperature and Nusselt numbers in the top, bottom, left and right sides of the channel. The flow and velocity lines are plotted.

In the isotherm diagram, Figs.5, 6 and 7 the maximum temperature in the wall is high. The number gets smaller as it approaches the bottom. Compared to Figs. 5, 6 and 7, the slope of temperature that changes at the beginning of the channel is higher for the peak horizontal position and at the end of the channel for a square vertical state.

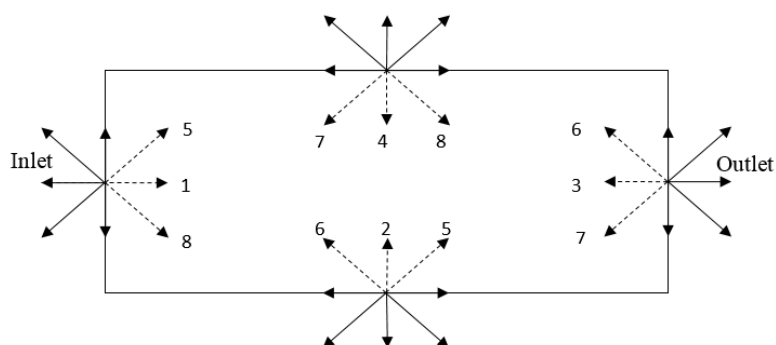


Fig. 4. Distribution functions at the boundaries of the domain.

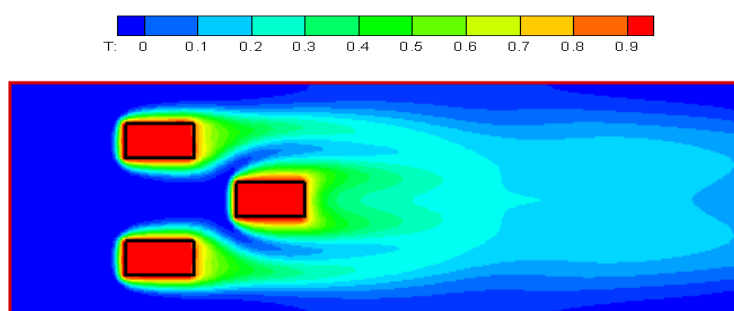


Fig. 5. 2Dimensional temperature distribution of channel with horizontal rectangular obstacle.

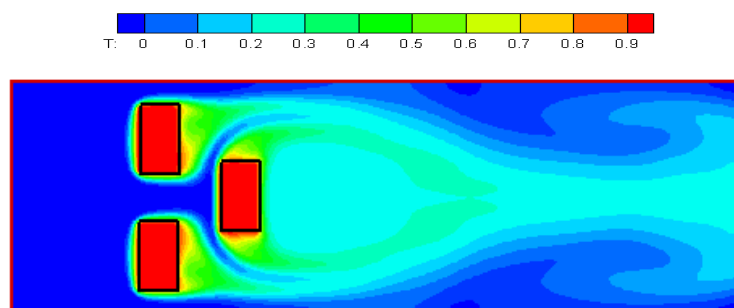


Fig. 6. 2Dimensional temperature distribution of channel with vertical rectangular obstacle

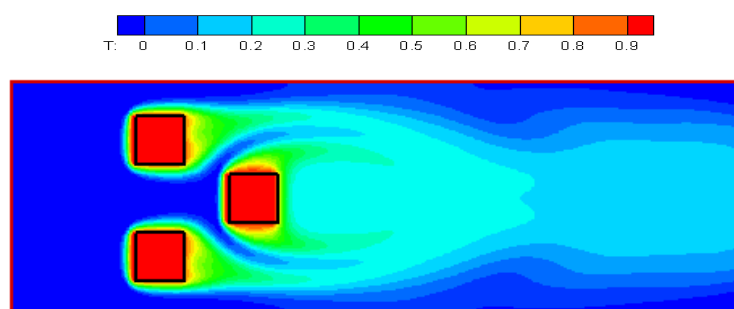
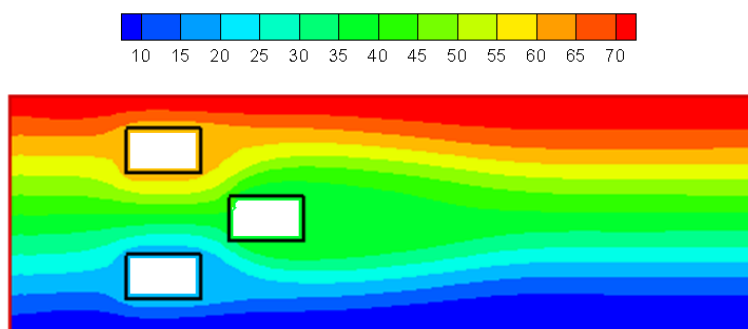


Fig. 7. 2Dimensional temperature distribution of channel with square obstacle



In the study of flow lines for all three states, Fig.8, 9 and 10 in distancing from surfaces are more powerful than in streamline and the variations of streamline in vertical mode are maximum and minimum in square mode



**Fig. 8. 2Dimensional streamline of channel with horizontal rectangular obstacle.**

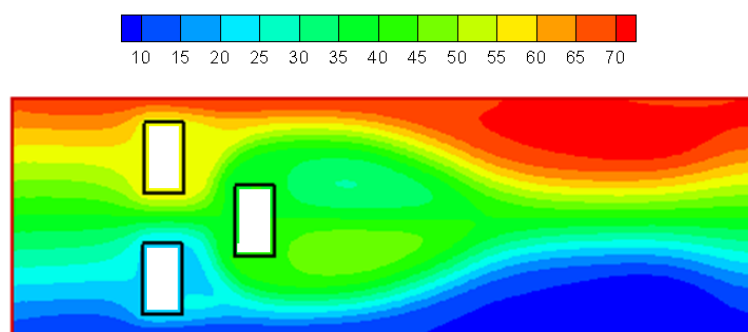


**Fig9. . 2Dimensional streamline of channel with vertical rectangular obstacle.**

Fig. 11, 12 and 13 show the study of vorticity lines in three states which are very similar to the figures of the streamlines.

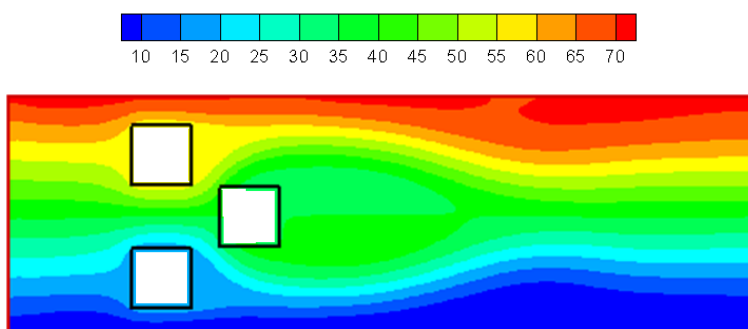


**Fig. 10. 2Dimensional streamline of channel with square obstacle.**

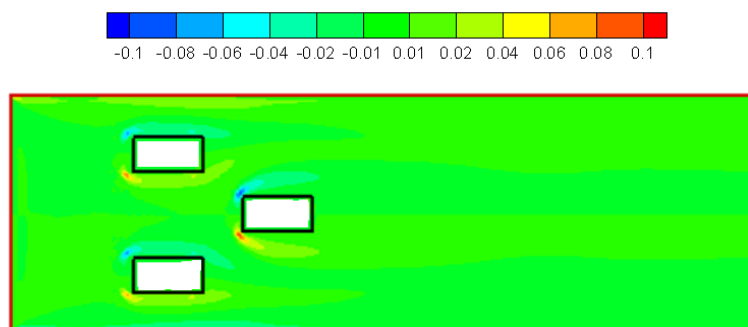


Fig 11. 2Dimensional vorticity of channel with horizontal rectangular obstacle.

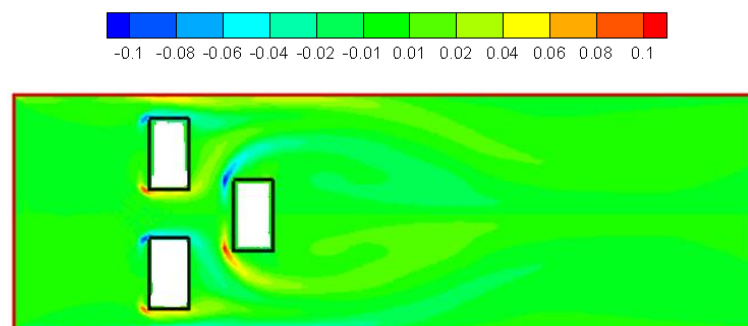


Fig. 12. 2Dimensional vorticity of channel with vertical rectangular obstacle

In the study of Nusselt number for the order of the 3 horizontal rectangles, first, the effect of Nusselt number changes along the rectangle length in the lower edge (from  $y=0$  to  $y=1$ ) is investigated in graph 1.

In graphs (1 to 12) given below, we have examined the Nusselt numbers all around the middle obstacle (center of channel), which values of  $Y$  in  $Nu$  left and  $Nu$  right are increasing from the bottom to top and for  $Nu$  up and  $Nu$  down and from the left to the right changes from zero to one.

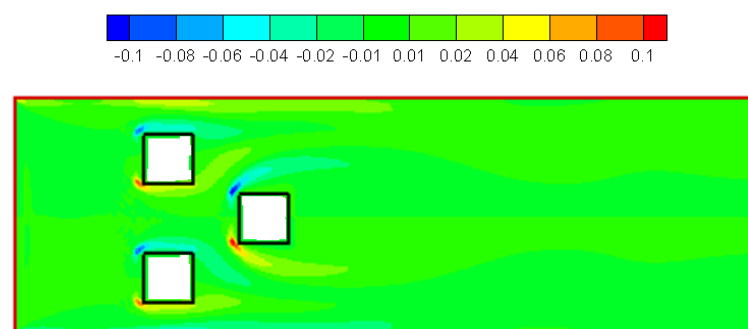
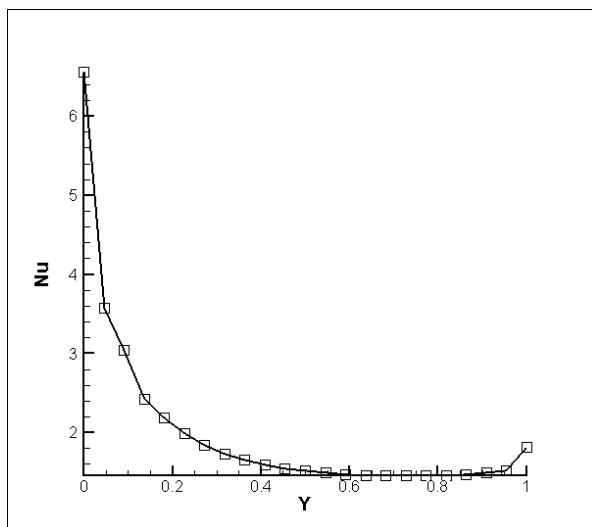
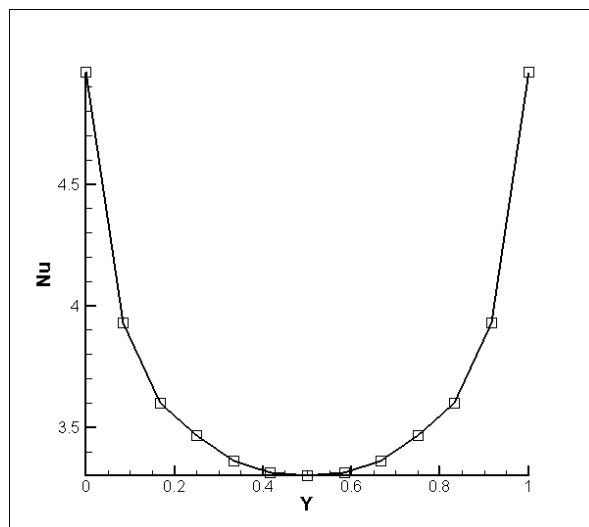


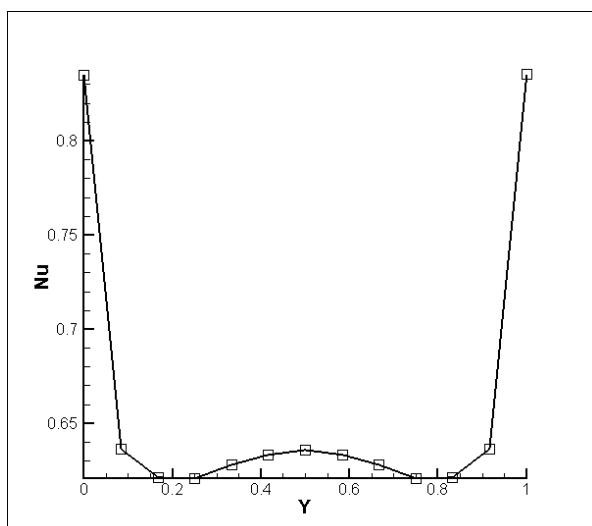
Fig. 13. 2Dimensional vorticity of channel with square obstacle



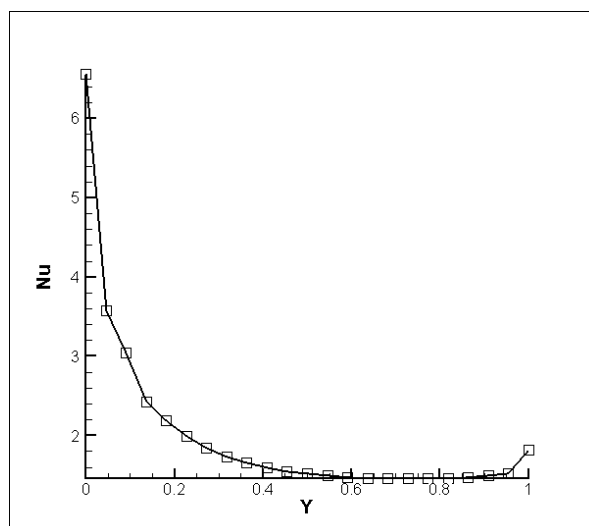
**Graph1. 2Dimensional Nu down for of channel with horizontal rectangular obstacle**



**Graph2. 2Dimensional. Nu left for of channel with horizontal rectangular obstacle**



**Graph3. 2Dimensional Nu right for of channel with horizontal rectangular obstacle**

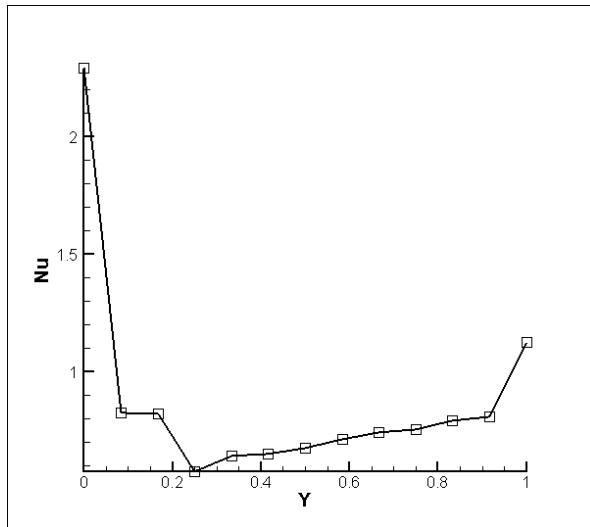


**Graph4. 2Dimensional. Nu up for of channel with horizontal rectangular obstacle**

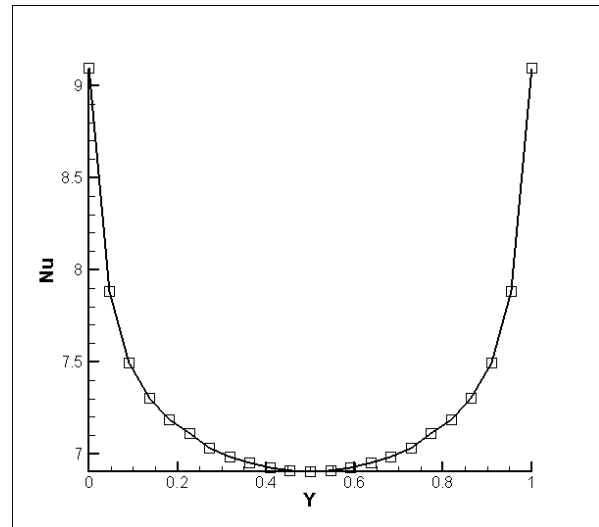
Then, we investigated the entrance edge of the horizontal rectangle in the graphs of the top 2 sides and the 3 vertical bottom edges of the graph 4 which there is a completely similar graph in Fig.1 and 4. And the maximum Nusselt number is at the beginning. And is near 1.6 around  $y=0.5$  till it jumps in the end around  $y=0.95$  and reaches 1.8.

This symmetry is found in the vertical rectangle for the graphs 5 and 8, except in this case the Nusselt number will reach 0.2 in  $y=0.25$  and then begins to grow and will reach 0.6 around  $y=0.9$  and it has a jump in the end which gets to 1.5. The difference between vertical and horizontal is that the Nusselt starts in 6 and ends to 2 in horizontal state but in horizontal state starts in 3 and ends in 1.4

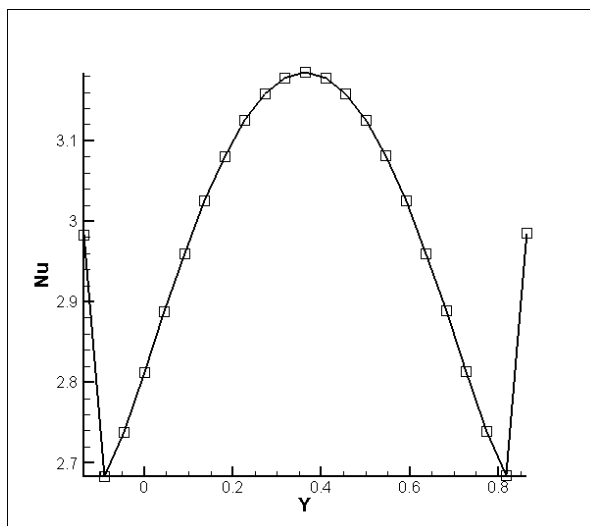
In entrance edge of the graph 2. Nusselt number starts from 4.95 in  $y=0$  and gets to its minimum of 3.3 in the middle of the edge.



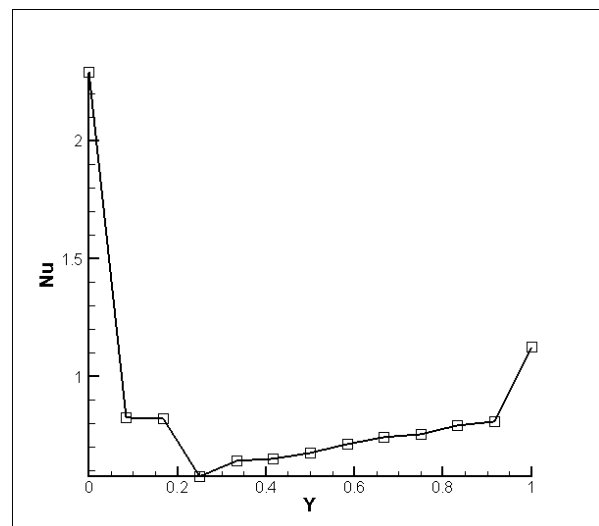
**Graph5. 2Dimensional Nu down for of channel with vertical rectangular obstacle**



**Graph6. 2Dimensional. Nu left for of channel with vertical rectangular obstacle**



**Graph7. 2Dimensional Nu right for of channel with vertical rectangle obstacle**



**Graph8. 2Dimensional Nu up for of channel with vertical rectangle obstacle**

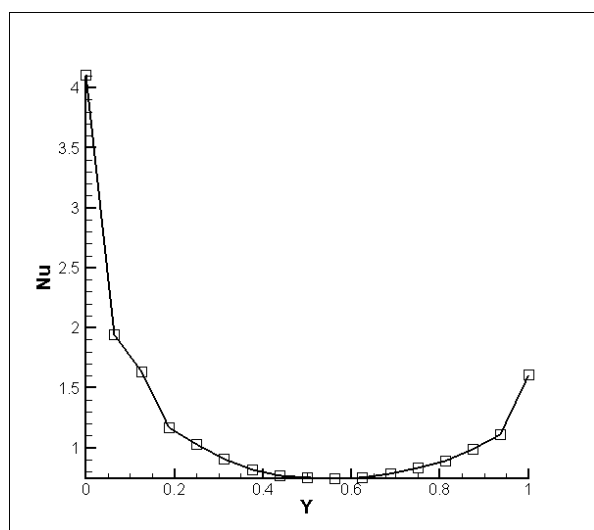
Then, symmetrically increases with the first half, but for the vertical side of the last horizontal rectangle the Nusselt number starts from 0.85 in  $y=0$  and reaches to 0.62 in  $y=0.2$  and swings in range of 0.62 to 0.64 for  $0.2 < y < 0.8$ . And symmetrically reaches 0.85 for  $y=1$ . Graph 3.

For a vertical rectangle at the beginning of the graph 6, the Nusselt number starts from 9.1 for  $y=0$  and decreases to 6.9 in  $y=0.5$  and continues symmetrically with the first half till gets to 9.1 in  $y=1$  which is only very similar in shape to the

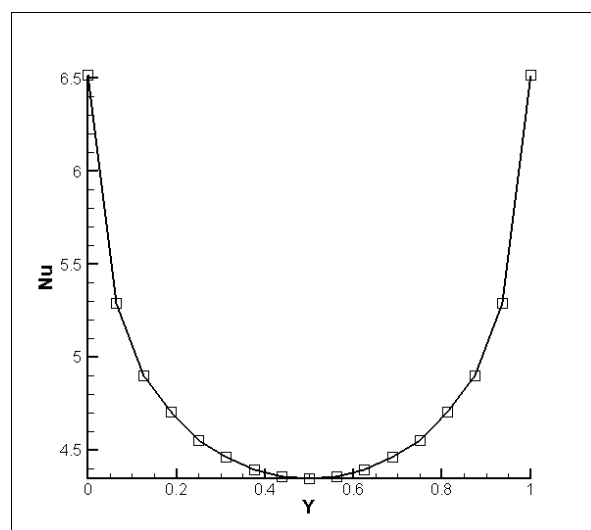
Entrance edge of the horizontal rectangle. In the last edge of the graph 7 in  $y=0$ , the Nusselt number starts from 2.98 and decreases to its least 2.65 in  $y=0.1$  and continues with incremental trend increases to around 3.06 in  $y=0.4$  and symmetrically gets to 2.65 in  $y=0.8$  again. And also

symmetrically continues to 2.98 in  $y=1$  which the shape of its graph is very different from the horizontal rectangle.

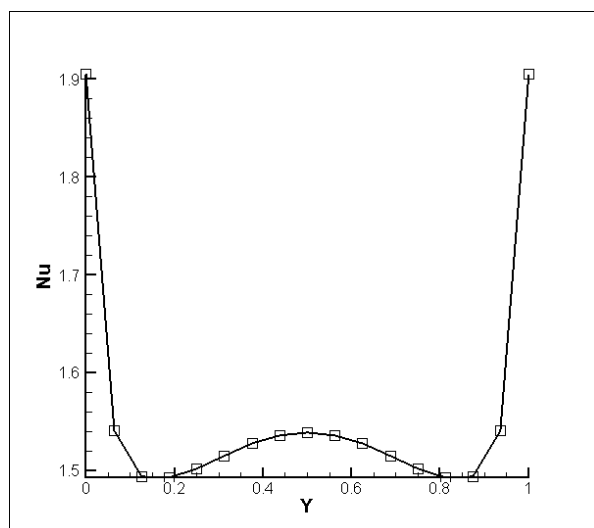
In square mode both Nusselt number and its variations are between vertical and horizontal state. Thus, the Nusselt number is in the vertical rectangle and then the square and then for the horizontal state which naturally applies to heat transfer (graphs 9-12).



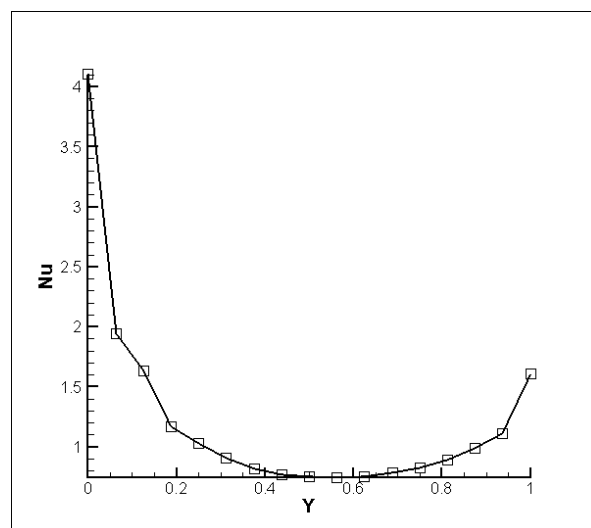
**Graph9. 2Dimensional Nu down for of channel with square obstacle**



**Graph10. 2Dimensional. Nu left for obstacle of channel with square**



**Graph11. 2Dimensional Nu right for of channel square obstacle**



**Graph12. 2Dimensional Nu up for of channel with square obstacle**

#### 4- Conclusion

In general, the maximum amount of Nusselt - as a result is the maximum heat transfer rate - related to the vertical, rectangular and then square state and the minimum is horizontal rectangular. Table 3. If we consider a square state with a vertical rectangle, two of which is  $a=b$ . "a" is the length and "b" is the width of the rectangle. Compared to the vertical rectangular, the greater  $a>b$  the heat transfer rate increases. Studies show that the upper and lower sides of the maximum Nusselt number and heat transfer are inversely proportional to the average Nusselt. Thus for the horizontal rectangle, square, vertical rectangle is the maximum. And vorticity lines in three states are very similar to the figures of the streamlines.

**Table 3**

	Nu (left)	Nu (Right)	Nu (down)	Nu (up)	Nu (Average)
Rectangular vertical	7.666446	3.111696	0.9523527	0.9522507	3.170686
Rectangular horizontal	4.047167	0.7153693	2.101064	2.100124	2.240931
square	5.169253	1.660424	1.302724	1.302881	2.358820

## References

- 1) R. Mittal, and S. Balachandar, Direct Numerical Simulation of flow past elliptic cylinders, Journal of Computational Physics, 124(1996) 351-367.
- 2) B. Sharman, F. S. Lien, L. Davidson and C. Norberg, Numerical predictions of low Reynolds number flows over two tandem circular cylinders, Int. J. Numer. Meth. Fluids 47(2005) 423-447.
- 3) D. Arumuga Perumal, Gundavarapu V.S. Kumar and Anoop K. Dass, Lattice Boltzmann Simulation of Viscous Flow past Elliptical Cylinder, J. CFD letters, 4(2012) 127-139.
- 4) K. Shintani, A. Umemura and A. Takano, Low-Reynolds-number flow past an elliptic cylinder, Journal of Fluid Mechanics, 136(1983) 277-289.
- 5) F. J. Higuera, J. Jimenez, Boltzmann approach to lattice gas simulation. Europhys. Lett. 9(1989) 663-668.
- 6) POURZIAEI ARABAN Hadi, Alinejad, Javad, Domairry Ganji, Davood, (2020) Control temperature fluctuations in two-phase CuO-water nanofluid by transfiguration of the enclosures. Thermal Science(2020)<https://doi.org/10.2298/TSCI200524334P>
- 7) Y. Chen, H. Ohashi, M. A. Akiyama, Thermal lattice Bhatnagar-Gross-Krook model without nonlinear deviations in macro dynamic equations. Phys. Rev. E50 (1994) 2776-2783.
- 8) P. Pavlo, G. Vahala, L. Vahala, M. Soe, Linear-stability analysis of thermo-lattice Boltzmann models. J. Comput. Phys. 139(1998)79-91.
- 9) B. Crouse, M. Krafczyk, S. Kuhner, E. Rank, C. Van Treeck, Indoor air flow analysis based on lattice Boltzmann methods. Energy Build 34(2002)941-949.
- 10) A. D'Orazio, M. Corcione, G. P. Cielata, Application to natural convection enclosed flows of a lattice Boltzmann BGK model coupled with a general purpose thermal boundary condition. Int. J. Thermal Sci. 43(2004)575-586.
- 11) A. Korichi, and L. Oufer, Numerical heat transfer in a rectangular channel with mounted obstacles on the upper and lower walls. Int. J. Thermal Sciences, 44(2005) 644-655.

- 12) G. Juncu, A numerical study of momentum and forced convection heat transfer around two tandem circular cylinders at low Reynolds numbers. Part II; Forced convection heat transfer. *Int. J. Heat Mass Transfer*, 50(2007) 3799–3808.
- 13) M. Farhadi, K. Sedighi, and M. M. Madani, Convective cooling of tandem heated squares in a channel. *Proc. IMechE, PartC: J. Mechanical Engineering Science*, 223(2009)965–978.
- 14) M. Mohammadi Pirouz, M. Farhadi, K. Sedighi, H. Nemati, E. Fattahi, Lattice Boltzmann simulation of conjugate heat transfer in a rectangular channel with wall-mounted obstacles. *J. Scientia Iranica B*, 18(2011)213–22.
- 15) - Domairry Ganji, Davood, Peiravi, Mohammad Mohsen, and Abbasi, Morteza. (2015). Evaluation of the heat transfer rate increases in retention pools nuclear waste. *International Journal of Nano Dimension*. Vol. 6. No. 4. 385-398.
- 16) Peiravi, Mohammad Mohsen, Alinejad, Javad, Domairry Ganji, Davood, and Maddah, Soroush. (2019). Numerical study of fins arrangement and nanofluids effects on three-dimensional natural convection in the cubical enclosure. *Transp Phenom Nano Micro Scales*. Vol. 7. No. 2. 97-112.
- 17) Peiravi, Mohammad Mohsen and Alinejad, Javad. (2020). Hybrid conduction, convection and radiation heat transfer simulation in a channel with rectangular cylinder. *Journal of Thermal Analysis and Calorimetry*. Vol. 140. No. 6. 2733-2747.
- 18) Alinejad, Javad and Peiravi, Mohammad Mohsen. (2020). Numerical analysis of secondary droplets characteristics due to drop impacting on 3d cylinders considering dynamic contact angle. *Meccanica*. Vol. 55. No. 10. 1975–2002.
- 19) Peiravi, Mohammad Mohsen, Alinejad, Javad, Domairry Ganji, Davood, and Maddah, Soroush. (2019). 3D optimization of baffle arrangement in a multi-phase nanofluid natural convection based on numerical simulation. *International Journal of Numerical Methods for Heat and Fluid Flow*. Vol. 30. No. 5. 2583-2605
- 20) B. Chopard, and P. O. Luthi, Lattice Boltzmann computations and applications to physics. *Theoret. Comput. Phys*. 217(1999)115–130.
- 21) R. R. Nourgaliev, T. N. Dinh, T. G. Theofanous, and D. Joseph, The lattice Boltzmann equation method: theoretical interpretation, numerics and implications. *Int. J. Multiph. Flow* 29(2003)117–169.
- 22) D. Yu, R. Mei, L. S. Luo, and W. Shyy, Viscous flow computations with the method of lattice Boltzmann equation. *Progr. Aerospace. Sci*. 39(2003)329–367.
- 23) A. A. Mohammad, *Applied Lattice Boltzmann Method for Transport Phenomena Momentum Heat Mass Transfer*. University of Calgary Press, Calgary (2007).
- 24) D. M. Aghajani, M. Farhadi, and K. Sedighi, Effect of heater location on heat transfer and entropy generation in the cavity using the lattice Boltzmann method. *Heat Transfer Research*, 40(2009)521–536.
- 25) A. Mezrhab, M. Jami, C. Abid, , M. Bouzidi, and P. Lallemand, Lattice Boltzmann modeling of natural convection in an inclined square enclosure with partitions attached to its cold wall. *Int. J. Heat Fluid Flow* 27(2006)456–465.
- 26) X. He, and L. S. Luo, Lattice Boltzmann model for the incompressible Navier–Stokes equations. *J. Stat. Phys*. 88(1997)927–944.

- 27) N. Thürey, and U. Rüde, Stable free surface flows with the lattice Boltzmann method on adaptively coarsened grids. *Comput. Vis. Sci.* 12(2009)247–263.
- 28) Z. L. Guo, Ch. Zheng, B. C. Shi, An extrapolation method for boundary conditions in lattice Boltzmann method, *Phys. Fluids* 14(6)(2002) 2007-2010.
- 29) J. Park, K. Kwon, H. Choi, Numerical solutions of flow past a circular cylinder at Reynolds number up to 160, *KSME Int. J.* 12(1998)1200.
- 30) D. Sucker, H. Brauer, Fluidodynamik bei der angestromten Zilindern, *Warme Stoffübertragung* 8(1975)149.
- 31) W. A. Khan, J. R. Culham, and M. M. Yovanovich, Fluid Flow Around and Heat Transfer from Elliptical Cylinders: Analytical Approach, *J. Thermophysics Heat Transfer*, 19(2005)178-185.
- 32) Johan Hoffman, Efficient computation of mean drag for the subcritical flow past a circular cylinder using General Galerkin G2, *Int. J. numerical methods in fluids* 59.11 (2009)1241-1258.
- [33] Y. Shimizu and Y. Tanida, Fluid forces acting on cylinders of rectangular cross-section, *Trans. JSME B*, 44 (384) (1978)2699-2706.
- [34] A. Okajima, Numerical analysis of flow around an Oscillating cylinder, *Proc.sixth Int.Conf. On flow induced vibration*, London, U.K (1995)159-166.